AIAA-2002-1427

CONSTITUTIVE MODELING OF NANOTUBE-REINFORCED POLYMER COMPOSITES [1]

G.M. Odegard[*], T.S. Gates[†], K.E. Wise[*]
NASA Langley Research Center, Hampton, Virginia

Abstract

In this study, a technique is presented for developing constitutive models for polymer composite systems reinforced with single-walled carbon nanotubes (SWNT). Because the polymer molecules are on the same size scale as the nanotubes, the interaction at the polymer/nanotube interface is highly dependent on the local molecular structure and bonding. At these small length scales, the lattice structures of the nanotube and polymer chains cannot be considered continuous, and the bulk mechanical properties can no longer be determined through traditional micromechanical approaches that are formulated by using continuum mechanics. It is proposed herein that the nanotube, the local polymer near the nanotube, and the nanotube/polymer interface can be modeled as an effective continuum fiber using an equivalent-continuum modeling method. The effective fiber serves as a means for incorporating micromechanical analyses for the prediction of bulk mechanical properties of SWNT/polymer composites with various nanotube shapes, sizes, concentrations, and orientations. As an example, the proposed approach is used for the constitutive modeling of two SWNT/LaRC-SI (with a PmPV interface) composite systems, one with aligned SWNTs and the other with three-dimensionally randomly oriented SWNTs. The Young's modulus and shear modulus have been calculated for the two systems for various nanotube lengths and volume fractions.

Introduction

In the last five years, nano-structured, non-metallic materials have spurred considerable interest in the materials community partly due to their potential for large gains in mechanical and physical properties as compared to standard structural materials. In particular, carbon nanotube-reinforced polymer composites may provide order-of-magnitude increases in strength and stiffness when compared to typical carbon-fiber reinforced polymeric composites. In order to facilitate the development of nanotube-reinforced polymer composites, constitutive relationships must be developed that predict the bulk mechanical properties of the composite as a function of molecular structure of the polymer, nanotube, and polymer/nanotube interface.

For simplicity, it is desirable to couple an equivalent-continuum model of a nanotube/polymer composite with established micromechanical models to describe the mechanical behavior. As outlined by McCullough,[1,2] numerous micromechanical models have been developed to predict the macroscopic behavior of composite materials reinforced with typical reinforcement fibers. These micromechanical models assume that the fiber, matrix, and sometimes, the interface, are continuous materials and the constitutive equations for the bulk composite material are formulated based on assumptions of continuum mechanics. However, a typical SWNT may have a diameter of approximately $1\text{-}10\times10^{-9}$ meters compared to the typical carbon-fiber diameter of 50×10^{-6} meters. Even though a limited number of studies have addressed the applicability of micromechanics to nanotube-reinforced polymer composites,[3,4] it appears that the direct use of micromechanics for nanotube composites is complicated by effects associated with the significant size difference between a nanotube and a typical carbon fiber, as described below.

Atomistic simulation is one approach that can be used to investigate behavior of materials at the nanometer length scale. Recently, Wise and Hinkley[5] used molecular dynamics simulations to address the polymer/SWNT material response for a SWNT surrounded by polyethylene molecules. They predicted that the local changes in the polymer molecular structure and the non-functionalized polymer/SWNT interface are on the same length-scale as the width of the nanotube. The magnitude of this localized effect is

[*] Staff Scientist, ICASE
[†] Senior Materials Research Engineer, Mechanics and Durability Branch. Associate Fellow, AIAA

not presently known and needs to be accurately modeled to ensure that the full load-transfer capabilities of the polymer/SWNT composite is accounted for in both stiffness and strength calculations.

The first step towards calculation of bulk stiffness and strength is to establish a constitutive model that can be used in a continuum mechanics formulation. A fundamental assumption in continuum mechanics is that the mass, momentum, and energy can be represented in a mathematical sense by continuous functions, that is, independent of length scale.

In this paper, a technique for developing constitutive models for SWNT-reinforced polymer composite materials is proposed which is based on extensions of the equivalent-continuum modeling technique developed by Odegard *et al.*[6] The modeling technique takes into account the discrete nature of the atomic interactions at the nanometer length scale and the interfacial characteristics of the nanotube and the surrounding polymer matrix. After the constituent materials used in this paper are discussed in detail, the development of the constitutive model using the presented technique is described. First, a model of the molecular structure of the nanotube and the adjacent polymer chains is established by using the atomic structure that has been determined from molecular dynamics (MD) simulations. Second, an equivalent-continuum model is developed in which the mechanical properties are determined based on the force constants that describe the bonded and non-bonded interactions of the atoms in the molecular model and reflect the local polymer and nanotube structure. Finally, the equivalent-continuum model is used in micromechanical analyses to determine the bulk constitutive properties of the SWNT/polymer composite with aligned and random nanotube orientations and with various nanotube lengths and volume fractions.

Constituent materials

The constitutive model developed in this study is for a carbon nanotube/LaRC-SI composite with a PmPV interface. The properties of the constituent materials are described below.

Carbon nanotube

In 1991 Iijima[7] obtained transmission electron micrographs of elongated, nano-sized carbon particles that consisted of cylindrical graphitic layers, known today as carbon nanotubes. Because of their high inter-atomic bond strength and perfect lattice structure, a Young's modulus as high as 1 TPa and a tensile strength approaching 100 GPa have been measured for single-walled carbon nanotubes (SWNT).[8] These properties, in addition to their relatively low density, make SWNT an ideal candidate as a reinforcing constituent.

Nanotube/polymer interface

In a molecular dynamics study of SWNT/polymer materials, Frankland *et al.*[9] addressed the effects of covalent bonds at the SWNT/polymer interface. They have shown that for nanotube/polyethylene composites there is a one to two order-of-magnitude increase in the interfacial shear strength for composites with covalent bonding between the nanotube and adjacent polymer molecules relative to systems without the covalent bonds. However, other studies[10,11] have shown that because the covalent bonding may significantly affect the properties of the nanotube itself, it is desirable to increase the load transfer between the nanotube and polymer by using improved non-covalent bonding methods. For example, it has been shown that PmPV molecules [poly(m-phenylenevinylene) substituted with octyloxy chains] naturally wrap around carbon nanotubes in a helical pattern.[11] This wrapping allows for an improved nanotube/polymer molecule interaction through non-covalent bonded interactions, and thus improved load transfer at the nanotube/polymer interface, compared to those found with traditional structural polymers. Because the PmPV polymer molecules will likely entangle themselves with neighboring structural polymer molecules (such as polyimides and epoxies), the PmPV can be used as a highly effective interface between the nanotube and structural polymer, and is used as the interface in the present study.

Polymer

The polymer used in this study is LaRC-SI, a thermoplastic polyimide that has been shown to have good mechanical properties for various processing and testing conditions.[12-15] The properties of LaRC-SI used in this study have been taken from Whitley *et al.*[15] for LaRC-SI with a 3% stoichiometric imbalance at room temperature. The Young's modulus and Poisson's ratio are 3.8 GPa and 0.4, respectively.

Molecular potential energy

The bonded and non-bonded interactions of the atoms in a molecular structure can be quantitatively described by using molecular mechanics. The forces that exist for each bond, as a result of the relative atomic positions, are described by the force field. These forces contribute to the total molecular potential energy of a molecular system. In general, the molecular potential energy for a nano-structured material is described by the sum of the individual energy contributions in the molecular model:[16]

$$E^m = \sum_{bond} E^{\rho} + \sum_{bond} E^{\theta} + \sum_{bond} E^{\tau} + \sum_{bond} E^{\omega} + \sum_{bond} E^{nb} \quad (1)$$

where E^{ρ}, E^{θ}, E^{τ}, and E^{ω} are the energies associated with bond stretching, angle variation, torsion, and inversion, respectively, and E^{nb} is the energy of the non-bonded interactions, which includes van der Waals and electrostatic effects (Fig. 1). The individual energy contributions are summed over the total number of corresponding interactions in the molecular model. Various functional forms may be used for these energy terms depending on the particular material and loading conditions considered.[16]

In this study, the total molecular potential energy of the molecular model is taken to be:

$$E^m = \sum_a K_a^{\rho} \left(\rho_a - \mathrm{P}_a\right)^2 + \sum_a K_a^{\theta} \left(\theta_a - \Theta_a\right)^2 + \sum_a D_a^{\mathrm{IJ}} \left[\frac{1}{2} \left(\frac{\rho_a^{\mathrm{IJ}}}{\rho_a} \right)^{12} - \left(\frac{\rho_a^{\mathrm{IJ}}}{\rho_a} \right)^{6} \right] \quad (2)$$

where the terms P_a and Θ_a refer to the undeformed interatomic distance of bond number a and the undeformed bond-angle number a, respectively. The quantities ρ_a and θ_a are the distance and bond-angle after stretching and angle variance, respectively. The symbols K_a^{ρ} and K_a^{θ} represent the force constants associated with the stretching and angle variance of bond and bond-angle number a, respectively. The well depth and natural van der Waals distance for interaction a are given by, respectively:

$$D_a^{\mathrm{IJ}} = \sqrt{D_a^{\mathrm{I}} \cdot D_a^{\mathrm{J}}}$$
$$\rho_a^{\mathrm{IJ}} = \sqrt{\rho_a^{\mathrm{I}} \cdot \rho_a^{\mathrm{J}}} \quad (3)$$

where the superscripts I and J denote the two atoms involved in an individual van der Waals interaction. Only the bond stretching, bond-angle variation, and van der Waals parameters were considered in Eq. (2) since the remaining energy terms in Eq. (1) were found to have a negligible contribution to the total molecular potential energy. The molecular structure of a single unit of the PmPV molecule is shown in Fig. 2. The values of the force constants, well depths, and natural van der Waals distances, equilibrium bond lengths, and equilibrium bond angles associated with the atoms shown in Fig. 2 are listed in Tables 1-3.

Molecular dynamics simulation

The Molecular Dynamics (MD) technique has become an effective tool for studying the physics of condensed matter systems in which the forces acting on particles in a defined cell are calculated and the classical Newtonian equations of motion are solved numerically.[17-19] In general, each particle is allowed to interact with all the other particles in the simulation.

In the present study, a MD simulation was used to generate the equilibrium structure of the composite system, which consisted of a (6,6) single-walled nanotube and five PmPV oligimers, each ten repeating units in length. The initial structure was constructed by placing the nanotube at the center of the MD cell, and by inserting the PmPV molecules at random, non-overlapping positions within the MD cell. This sample was equilibrated for approximately 500ps at 800K and 500 atm of hydrostatic pressure to relax the initial configuration and compress the system to an appropriate density. This initial procedure was followed by an additional 500ps of simulation at 300K and 1 atm of pressure. By the end of the final equilibration run, the total energy and density had stabilized. No constraints were placed on the periodic MD cell shape or size.

The parameters used in the MD simulation are listed in Tables 1-3, with the atom labels defined in Fig. 2. All parameters, other than those involving the oxygen atom were taken from the OPLS-AA force field developed by Jorgensen and coworkers.[20-22] Parameters for the ether linkage were adapted from the MM3 force field.[23-25] All simulations were carried out with the TINKER® 3.8[26] molecular modeling package. The resulting molecular model is shown on the left side of Fig. 3.

Equivalent-continuum modeling

The equivalent-continuum model of the composite material can be developed based on the equilibrium molecular structure obtained with the MD simulation by using the methods of Odegard *et al.*[6] This approach relies on an equivalent-continuum modeling technique that is used to predict the bulk mechanical behavior of nano-structured materials. In summary, the method consists of two major steps. First, a suitable representative volume element (RVE) of the nano-structured material is chosen. The RVE of a typical nano-structured material is on the nanometer length scale, therefore, the material of the RVE is not continuous, but is an assemblage of many atoms. Interaction of these atoms is described in terms of molecular mechanics force constants, which are known for most atomic structures.[16] Second, an equivalent-continuum model of the RVE is developed in which the

total strain energy in the molecular and equivalent-continuum models, under identical loading conditions, is equal. The effective mechanical properties, or the effective geometry, of the equivalent-continuum is then determined from equating strain energies.

For the most general approach, an equivalent-truss model of the RVE may be developed as an intermediate step to link the molecular and equivalent-continuum models. Each atom in the molecular model is represented by a pin-joint, and each truss element represents an atomic bonded or non-bonded interaction. The moduli of the truss elements are based on the molecular mechanics force constants. Therefore, the total molecular potential energy of the molecular model and the strain energy of the equivalent-truss are equal for the same loading conditions.

Truss model

In traditional molecular models, the atomic lattice has been viewed as an assemblage of discrete masses that are held in place with atomic forces that resemble elastic springs.[27] The mechanical analogy of this model is a pin-jointed truss model in which each truss member represents either a bonded or non-bonded interaction between atoms. Therefore, the truss model allows the mechanical behavior of the nano-structured system to be accurately modeled in terms of displacements of the atoms. The deformation of each bonded or non-bonded interaction corresponds to the axial deformation of the corresponding truss element.

The total mechanical strain energy, E^t, of the truss model is:

$$E^{\mathrm{t}} = \sum_b \sum_a \frac{A_a^b Y_a^b}{2R_a^b}\left(r_a^b - R_a^b\right)^2 \tag{4}$$

where A_a^b and Y_a^b are the cross-sectional area and Young's modulus of rod a of truss member type b, respectively. The term $r_a^b - R_a^b$ is the stretching of rod a of truss member type b, where R_a^b and r_a^b are the undeformed and deformed lengths of the truss elements, respectively.

In order to represent the mechanical behavior of the molecular lattice model with the truss model, Eq. (4) must be equated with Eq. (2) in a physically meaningful manner. Both equations are the sum of energies for particular degrees of freedom. The main difficulty in the substitution is specifying Eq. (4), which has stretching terms only, for Eq. (2), which also has bond-angle variance and van der Waals terms.

It was shown by Odegard *et al.*[6] that for small deformations, the Young's moduli of the rods representing primary bonds and the bond-angle variance interactions may be determined as a function of the force constants:

$$Y_a^{\alpha} = \frac{2K_a^{\rho}R_a^{\alpha}}{A_a^{\alpha}} \tag{5}$$

$$Y_a^{\beta} = \frac{32K_a^{\theta}}{A_a^{\beta}R_a^{\beta}}\left(\sin\frac{\Theta_a}{2}\right)^2 \tag{6}$$

where K_a^{ρ}, K_a^{θ}, Θ_a are the same parameters associated with Eq. (2), and the superscripts α and β indicate primary bonding and bond-angle variance interactions, respectively.

Upon examination of Eq. (2), it is clear that the energy associated with van der Waals interactions is highly non-linear with respect to interatomic distance. The determination of the Young's moduli of truss elements that represent van der Waals interactions is complicated by accounting for this non-linearity and the large range of values for the interatomic distance of the interacting atoms in an equilibrium configuration. Therefore, linear relationships for the Young's modulus, such as those given by Eqs. (5) and (6), are not realistic for the van der Waals interactions.

To address this problem, the energy associated with the van der Waals interaction given in Eq. (2) and the strain energy of a truss element given by Eq. (4) were equated. The Young's modulus that represents the mechanical stiffness of a van der Waals interaction is given by:

$$Y_a^{\delta} = \frac{2\rho_a^{\mathrm{IJ}}D_a^{\mathrm{IJ}}}{A_a^{\delta}\left(\rho_a - \rho_a^{\mathrm{IJ}}\right)^2}\left[\frac{1}{2}\left(\frac{\rho_a^{\mathrm{IJ}}}{\rho_a}\right)^{12} - \left(\frac{\rho_a^{\mathrm{IJ}}}{\rho_a}\right)^{6}\right] \tag{7}$$

where the superscript δ indicates van der Waals bonding. Clearly, the Young's modulus is highly dependent on the interatomic spacing. However, because of the difficulty of assigning an individual Young's modulus value for every van der Waals interaction in a nano-structured material, discrete values of Young's modulus may be approximated for ranges of interatomic spacing for each combination of atoms based on Eq. (7). The process for establishing these ranges is discussed below.

To implement the resultant equivalent-truss structure, a finite element model was developed by using ANSYS® 6[28] (Fig. 3). Each element (LINK8) was a three-dimensional pin-jointed truss element with six degrees of freedom (three displacement components on each end) that represented a single atomic interaction. Each node corresponded to an atom in the

equilibrium structure of the molecular model. A total of 14,501 elements and 1818 nodes were used in the model.

Continuum model

With the equivalent-truss structure in place, the continuum model could be constructed. The geometry of the homogeneous, equivalent-continuum RVE was assumed to be cylindrical, similar to that of the molecular and truss models (Fig. 3). With this approach, the mechanical properties of the solid cylinder were determined by equating the total strain energies of the equivalent-truss and equivalent-continuum models under identical loading conditions. Examination of the molecular model revealed that it was accurately described as having transversely isotropic symmetry, with the plane of isotropy perpendicular to the long axis of the nanotube. There are five independent material parameters required to determine the entire set of elastic constants for a transversely isotropic material. Each of the five independent parameters may be determined from a single boundary condition applied to both equivalent-truss and equivalent-continuum models. Once the mechanical properties of the equivalent-continuum RVE are determined, then the model may be used in subsequent micromechanical analyses as an effective fiber. The method employed in this study was adapted from the approach used by Hashin and Rosen[29] to determine elastic properties for fiber reinforced composite materials.

Effective fiber constitutive model

The constitutive relationship of the transversely isotropic equivalent-continuum RVE (which is referred to as the effective fiber throughout the remainder of the paper) is:

$$\sigma_{ij} = C^f_{ijkl}\varepsilon_{kl} \tag{8}$$

where σ_{ij} and ε_{kl} are the stress and strain components, respectively (i,j = 1,2,3), and C^f_{ijkl} are the elastic stiffness components of the effective fiber (denoted by superscript *f*). Alternatively, Eq. (8) can be simplified by using the usual contracted notation for the elastic stiffness components and transversely-isotropic symmetry:

$$\begin{aligned}
\sigma_{11} &= C^f_{11}\varepsilon_{11} + C^f_{12}\varepsilon_{22} + C^f_{12}\varepsilon_{33} \\
\sigma_{22} &= C^f_{12}\varepsilon_{11} + C^f_{22}\varepsilon_{22} + C^f_{23}\varepsilon_{33} \\
\sigma_{33} &= C^f_{12}\varepsilon_{11} + C^f_{22}\varepsilon_{22} + C^f_{23}\varepsilon_{33} \\
\sigma_{12} &= 2C^f_{44}\varepsilon_{12} \\
\sigma_{13} &= 2C^f_{44}\varepsilon_{13} \\
\sigma_{23} &= \left(C^f_{22} - C^f_{23}\right)\varepsilon_{23}
\end{aligned} \tag{9}$$

Five independent elastic properties may be chosen to describe the complete set of elastic stiffness components, namely, the elastic stiffness component, C^f_{11}, and four elastic parameters: transverse shear modulus, G^f_T, transverse bulk modulus (also known as the plane-strain bulk modulus), K^f_T, longitudinal shear modulus, G^f_L, and longitudinal Young's modulus, Y^f_L. The four elastic parameters are related to the elastic stiffness components by:

$$\begin{aligned}
G^f_T &= \frac{1}{2}\left(C^f_{22} - C^f_{23}\right) \\
K^f_T &= \frac{1}{2}\left(C^f_{22} + C^f_{23}\right) \\
G^f_L &= C^f_{44} \\
Y^f_L &= C^f_{11} - \frac{2C^{f\,2}_{12}}{C^f_{22} + C^f_{23}}
\end{aligned} \tag{10}$$

Conversely, the elastic stiffness components can be described in terms of the four elastic parameters:

$$\begin{aligned}
C^f_{44} &= G^f_L \\
C^f_{22} &= G^f_T + K^f_T \\
C^f_{23} &= K^f_T - G^f_T \\
C^f_{12} &= \left[K^f_T\left(C^f_{11} - Y^f_L\right)\right]^{\frac{1}{2}}
\end{aligned} \tag{11}$$

At this point, both the elastic parameters and the elastic stiffness components are unknown. These values are determined by applying five identical sets of boundary conditions to the equivalent-truss model and the effective fiber, and by subsequently equating the strain energies by adjusting the five independent elastic properties. Boundary conditions must be chosen to yield unique values for the independent elastic properties.

Boundary conditions

Fives sets of boundary conditions were chosen to determine each of the five independent elastic properties such that a single property could be independently determined for each boundary condition.

The displacements and tractions applied at the boundaries of the RVE are generalized, respectively, by:

$$u_i(S) = \varepsilon_{ij} x_j \tag{12}$$

$$T_i(S) = \sigma_{ij} n_j \tag{13}$$

where S is the bounding surface, x_j is defined in Fig. 3, and n_j are the components of the outward normal to S. The generalized total strain energy of the effective fiber is:

$$E^f = \frac{V}{2}\sigma_{ij}\varepsilon_{ij} = \frac{\pi D^2 L}{8}\sigma_{ij}\varepsilon_{ij} \tag{14}$$

where V, D, and L are the volume, diameter, and length of the effective fiber, respectively (Fig. 3). The boundary conditions and strain energies for each of the five independent elastic properties are listed in Table 4.

Boundary region

The displacements and tractions specified in Table 4 were applied to each node in the boundary region of the equivalent-truss model (indicated in Fig. 3), and the corresponding strain energies were calculated by summing the strain energies of each individual truss member in the RVE.

To determine the size of the boundary region, it was assumed that the range of the boundary region is related to the interatomic distance between the minimum non-bonded spacing found in the equilibrium structure to the maximum distance for which a positive-definite relationship exists between the force and displacement. It was also assumed that the contribution of the energies associated with van der Waals forces between atoms with a larger distance than this maximum were relatively small and could be neglected.

The recent MD simulation of a SWNT surrounded by polyethylene molecules performed by Wise and Hinkley,[5] predicted that the local changes in the polymer molecular structure and the non-functionalized polymer/SWNT interface are on the same length scale as the width of the nanotube. This recent study and the aforementioned assumptions led to the selection of a boundary region that extends to a radius of 0.9 nm measured from the center of the nanotube to the outer edge of the molecular model (Fig. 3). Within the 0.9 nm radius, the RVE includes the nanotube, nanotube/polymer interface, and polymer molecules immediately adjacent to the interface.

Material property summary

For an effective fiber diameter, D, of 1.8 nm and length, L, of 3.2 nm, the calculated values of the five independent parameters and the resulting elastic stiffness tensor components for the effective fiber calculated from Eq. (11) are listed in Table 5.

Micromechanical analysis

Constitutive models of the effective fiber/polymer composite may be developed with a micromechanical analysis by using the mechanical properties of the effective fiber and the bulk polymer matrix material. For the composite considered in this study, the PmPV molecules that were near the polymer/nanotube interface were included in the effective fiber, and it was assumed that the matrix polymer surrounding the effective fiber had mechanical properties equal to those of the bulk LaRC-SI resin. Because the bulk LaRC-SI polymer molecules and the polymer molecules included in the effective fiber are physically entangled, perfect bonding between the effective fiber and the surrounding polymer matrix was assumed.

The micromechanics-based Mori-Tanaka method[30,31] was used to predict the elastic mechanical properties of the composite material considered herein. For this method, the complete elastic stiffness tensor for the composite with transversely isotropic inclusions is given by:[32]

$$\mathbf{C} = \left(c_m \mathbf{C}^m + c_f \left\{\mathbf{C}^f \mathbf{A}^f\right\}\right)\left(c_m \mathbf{I} + c_f \left\{\mathbf{A}^f\right\}\right)^{-1} \tag{15}$$

where c_f and c_m are the fiber and matrix volume fractions, respectively, $\mathbf{I}$ is the identity tensor, $\mathbf{C}^m$ is the stiffness tensor of the matrix material, $\mathbf{C}^f$ is the stiffness tensor of the fiber, and $\mathbf{A}^f$ is the dilute mechanical strain-concentration tensor for the inclusion:

$$\mathbf{A}^f = \left[\mathbf{I} + \mathbf{S}\mathbf{C}^{m^{-1}}\left(\mathbf{C}^f - \mathbf{C}^m\right)\right]^{-1} \tag{16}$$

The tensor $\mathbf{S}$ is Eshelby's tensor, as given by Eshelby[33] and Mura.[34] The bracketed terms in Eq. (15) indicate inclusion orientation averaging of the bracketed tensor. For unidirectional-aligned inclusions, the orientation averaging in Eq. (15) is not necessary, and the resulting elastic stiffness components of the composite have transversely isotropic symmetry. For three-dimensional randomly oriented inclusions, the bracketed terms are given by Qui and Weng.[32] The resulting stiffness components for this case have isotropic symmetry.

For the effective fiber/polymer composite considered in the present study, the elastic stiffness components, volume fraction, length, and orientation of

the effective fiber were used for the inclusion properties in Eqs. (15) and (16). The effective fibers were assumed to have an ellipsoidal geometry for the Eshelby tensor in Eq. (16) so that both long and short effective fibers could be considered. The effective fiber length was adjusted by varying the inclusion aspect ratio while holding the diameter constant. The elastic stiffness components and volume fraction of LaRC-SI were used for the matrix properties. The overall composite stiffness was calculated for various effective fiber lengths and volume fractions for both cases of perfectly aligned and three-dimensional randomly oriented effective fibers (Fig. 4).

Results

In this section, the moduli of the effective fiber/polymer composite are presented in terms of nanotube length and nanotube volume fraction. While the nanotube and effective fiber lengths are equal, the nanotube volume fraction was determined to be 34% of the effective fiber volume fraction if it is assumed that the nanotube volume as a hollow cylinder with a wall thickness of 0.34 nm. For the aligned and random case, the longitudinal Young's and shear modulus were calculated. The properties of the random composite were calculated for nanotube lengths up to 200 nm. This maximum length was chosen based on the decreased likelihood of a nanotube remaining straight as the nanotube length exceeds 200 nm.

Figure 5 is a plot of the calculated Young's modulus and shear modulus for the aligned composite (longitudinal direction) and the random composite as a function of nanotube length, for a 1% nanotube volume fraction. These results indicate that the aligned orientation has higher Young's modulus than the random orientation for all nanotube lengths. Conversely, for the shear modulus, the random orientation provides greater stiffness than the aligned case for all nanotube lengths. For both aligned and random orientations, the shear modulus varies little for nanotube lengths exceeding 30 nm while the Young's modulus is continuously increasing as nanotube length increases. The rate of increase of Young's modulus for increasing nanotube length appears to decrease sharply at approximately 75 nm.

The longitudinal Young's modulus of the aligned composite is plotted in Figure 6 as a function of nanotube volume fraction for three nanotube lengths. Young's modulus increases with an increase in volume fraction, with the most pronounced rate of increase associated with nanotubes of length 50 nm or greater. The dependence of the longitudinal Young's modulus on the nanotube volume fraction becomes more linear as the nanotube length increases.

Figure 7 is a plot of the Young's modulus and the shear modulus for the random composite as a function of nanotube volume fraction, for three nanotube lengths. In general, an increase in nanotube volume fraction results in increased moduli values. For both the Young's and the shear moduli, increasing the volume fraction for the short nanotubes of length near 10 nm provides little to no improvement in stiffness. However, for nanotubes between 50 nm to 200 nm, an equivalent stiffness can easily be obtained by trading off a decrease in nanotube length for a small (2x or less) change in volume fraction. Increasing the nanotube length above 200 nm results in negligible increases in modulus.

Summary and conclusions

In this study, a method has been presented for linking atomistic simulations of nano-structured materials to continuum models of the corresponding bulk material. For a polymer composite system reinforced with single-walled carbon nanotubes (SWNT), the method provides the steps whereby the nanotube, the local polymer near the nanotube, and the nanotube/polymer interface can be modeled as an effective continuum fiber by using an equivalent-continuum model. The effective fiber retains the local molecular structure and bonding information, as defined by molecular dynamics, and serves as a means for linking the equivalent-continuum and micromechanics models. The micromechanics method is then available for the prediction of bulk mechanical properties of SWNT/polymer composites as a function of nanotube size, orientation, and volume fraction. The utility of this method was examined by modeling a SWNT/LaRC-SI composite with a PmPV interface. The elastic stiffness constants of the composite were determined for both aligned and three-dimensional randomly oriented nanotubes, as a function of nanotube length and volume fraction.

For the aligned composite at 1% nanotube volume fraction, stiffness will approach a maximum for nanotube lengths of 75 nm or greater. Lengths above this 75 nm range will also provide the most efficient increase in modulus for small changes in nanotube volume fraction. As length increases above 75 nm, there is a limiting value such that small gains are realized for lengths above approximately 200nm. This limiting value indicates that for nanotube lengths of approximately 200 nm, the efficiency of load transfer is nearly maximized. For long nanotubes (500 nm), the relationship between stiffness and volume fraction is linear, which resembles the usual rule-of-mixtures approximation for long-fiber composites. For short nanotubes (10 nm), the volume fraction must exceed 10% before stiffness gains can be obtained.

As for the aligned case, the 1% nanotube volume fraction, randomly oriented composite has maximum stiffness for nanotube lengths of approximately 75 nm or longer. However, unlike the aligned case, measurable shear-stiffness gains of at least 100% can be realized for small volume fractions.

For many nano-structured materials, the trade-offs between structure and property must be established before the material can be optimized for any given application. The method presented in this paper provides a means for parametrically exploring these structure-property relationships. The method is applicable to a wide range of problems that require the accuracy of atomistic level descriptions coupled with the general applicability of continuum-level models.

Acknowledgements

This work was performed while Dr. Odegard and Dr. Wise held National Research Council Research Associateship Awards at NASA Langley Research Center.

References

1. McCullough, R.L.: Micro-Models for Composite Materials - Continuous Fiber Composites. In: *Delaware Composites Design Encyclopedia-Volume 2: Micromechanical Materials Modeling*. J. M. Whitney and R. L. McCullough, eds. Lancaster, PA: Technomic Pub. Co., 1990, pp. 49-90.

2. McCullough, R.L.: Micro-Models for Composite Materials - Particulate and Discontinuous Fiber Composites. In: *Delaware Composites Design Encyclopedia-Volume 2: Micromechanical Materials Modeling*. J. M. Whitney and R. L. McCullough, eds. Lancaster, PA: Technomic Pub. Co., 1990, pp. 93-142.

3. Qian, D.; Dickey, E.C.; Andrews, R., and Rantell, T.: Load Transfer and Deformation Mechanisms in Carbon Nanotube-Polystyrene Composites. *Applied Physics Letters*. Vol. 76, No. 20, 2000, pp. 2868-2870.

4. Shaffer, M.S.P. and Windle, A.H.: Fabrication and Characterization of Carbon Nanotube/Poly(vinyl alcohol) Composites. *Advanced Materials*. Vol. 11, No. 11, 1999, pp. 937-941.

5. Wise, K. and Hinkley, J.: Molecular Dynamics Simulations of Nanotube-Polymer Composites. *American Physical Society Spring Meeting, April 12-16, 2001*. Seattle, WA; 2001.

6. Odegard, G.M.; Gates, T.S.; Nicholson, L.M., and Wise, K.E.: Equivalent Continuum Modeling of Nano-Structured Materials. NASA/TM-2001-210863.

7. Iijima, S.: Helical Microtubules of Graphitic Carbon. *Nature*. Vol. 354, 1991, pp. 56.

8. Edelstein, A.S. and Cammarata, R.C.: *Nanomaterials: Synthesis, Properties and Applications*. Bristol: Institute of Physics Publishing, 1996.

9. Frankland, S.J.V.; Caglar, A.; Brenner, D.W., and Griebel, M.: Reinforcement Mechanicism in Polymer Nanotube Composites: Simulated Non-Bonded and Cross-Linked Systems. *MRS Fall Meeting*. Boston, MA; 2000.

10. Chen, R.J.; Zhang, Y.; Wang, D., and Dai, H.: Noncovalent Sidewall Functionalization of Single-Walled Carbon Nanotubes for Protein Immobilization. *Journal of the American Chemical Society*. Vol. 123, 2001, pp. 3838-3839.

11. Star, A.; Stoddart, J.F.; Steuerman, D.; Diehl, M.; Boukai, A.; Wong, E.W.; Yang, X.; Chung, S.; Choi, H., and Heath, J.R.: Preparation and Properties of Polymer-Wrapped Single-Walled Carbon Nanotubes. *Angewandte Chemie International Edition in English*. Vol. 40, No. 9, 2001, pp. 1721-1725.

12. Nicholson, L.M.; Whitley, K.S.; Gates, T.S., and Hinkley, J.A.: Influence of Molecular Weight on the Mechanical Performance of a Thermoplastic Glassy Polyimide. *Journal of Materials Science*. Vol. 35, No. 24, 2000, pp. 6111-6122.

13. Nicholson, L.M.; Whitley, K.S., and Gates, T.S.: The Combined Influence of Molecular Weight and Temperature on the Physical Aging and Creep Compliance of a Glassy Thermoplastic Polyimide. *Mechanics of Time-Dependent Materials*. Vol. 5, 2001, pp. 199-227.

14. Nicholson, L.M.; Whitley, K.S., and Gates, T.S.: The Role of Molecular Weight and Temperature on the Elastic and Viscoelastic Properties of a Glassy Thermoplastic Polyimide. NASA/TM-2001-210664.

15. Whitley, K.S.; Gates, T.S.; Hinkley, J., and Nicholson, L.M.: Mechanical Properties of LaRC™ SI Polymer for a Range of Molecular Weights. NASA/TM-2000-210304.

16. Rappe, A.K. and Casewit, C.J.: *Molecular Mechanics Across Chemistry*. Sausalito, California: University Science Books, 1997.

17. Allen, M.P. and Tildesley, D.J.: *Computer Simulation of Liquids*. Oxford: Oxford University Press, 1987.

18. Rapaport, D.C.: *The Art of Molecular Dynamics Simulation*. Cambridge: Cambridge University Press, 1995.

19. Frankel, D. and Smit, B.: *Understanding Molecular Simulation: From Algorithms to Applications*. San Diego: Academic Press, 1996.

20. Duffy, E.M.; Kowalczyk, P.J., and Jorgensen, W.L.: Do Denaturants Interact with Aromatic Hydrocarbons in Water? *Journal of the American Chemical Society*. Vol. 115, No. 9271-9275, 1993, pp.

21. Jorgensen, W.L.; Madura, J.D., and Swenson, C.J.: Optimized Intermolecular Potential Functions for Liquid Hydrocarbons. *Journal of the American Chemical Society*. Vol. 106, 1984, pp. 6638-6646.

22. Jorgensen, W.L. and Severance, D.L.: Aromatic-Aromatic Interactions: Free Energy Profiles for the Benzene Dimer in Water, Chloroform, and Liquid Benzene. *Journal of the American Chemical Society*. Vol. 112, 1990, pp. 4768-4774.

23. Allinger, N.L.; Yuh, Y.H., and Lii, J.H.: Molecular Mechanics. The MM3 Force Field for Hydrocarbons. *Journal of the American Chemical Society*. Vol. 111, 1989, pp. 8551-8566.

24. Lii, J.H. and Allinger, N.L.: Molecular Mechanics. The MM3 Force Field for Hydrocarbons. 2. Vibrational Frequencies and Thermodynamics. *Journal of the American Chemical Society*. Vol. 111, 1989, pp. 8566-8575.

25. Lii, J.H. and Allinger, N.L.: Molecular Mechanics. The MM3 Force Field for Hydrocarbons. 3. The van der Waals' Potentials and Crystal Data for Aliphatic and Aromatic Hydrocarbons. *Journal of the American Chemical Society*. Vol. 111, 1989, pp. 8576-8582.

26. Ponder, J.W.: TINKER: Software Tools for Molecular Design, Ver. 3.6. Washington University School of Medicine, 1998.

27. Born, M. and Huang, K.: *Dynamical Theory of Crystal Lattices*. London: Oxford University Press, 1954.

28. Anonymous: ANSYS, Ver. 6. Canonsburg, PA: SAS IP, 2001.

29. Hashin, Z. and Rosen, B.W.: The Elastic Moduli of Fiber-Reinforced Materials. *Journal of Applied Mechanics*. Vol. 31, 1964, pp. 223-232.

30. Mori, T. and Tanaka, K.: Average Stress in Matrix and Average Elastic Energy of Materials with Misfitting Inclusions. *Acta Metallurgica*. Vol. 21, 1973, pp. 571-574.

31. Benveniste, Y.: A New Approach to the Application of Mori-Tanaka's Theory in Composite Materials. *Mechanics of Materials*. Vol. 6, 1987, pp. 147-157.

32. Qui, Y.P. and Weng, G.J.: On the Application of Mori-Tanaka's Theory Involving Transversely Isotropic Spheroidal Inclusions. *International Journal of Engineering Science*. Vol. 28, No. 11, 1990, pp. 1121-1137.

33. Eshelby, J.D.: The Determination of the Elastic Field of an Ellipsoidal Inclusion, and Related Problems. *Proceedings of the Royal Society of London, Series A*. Vol. A241, 1957, pp. 376-396.

34. Mura, T.: *Micromechanics of Defects in Solids*. The Hague: Martinus Nijhoff, 1982.

Table 1. Bond stretching parameters

Bond stretching	P (Å)	K^p (kcal/mole/ Å^2)
$C_t - C_t$	1.529	268.0
$C_t - H_t$	1.090	340.0
$C_t - O$	1.415	201.4
$C_a - O$	1.355	431.6
$C_a - C_a$	1.400	469.0
$C_a - H_a$	1.080	367.0
$C_a - C_v$	1.320	520.0
$C_v - C_v$	1.320	520.0
$C_v - H_v$	1.080	367.0

Table 2. Bond angle variation parameters

Bond-angle variation	Θ (deg)	K^{θ} (kcal/mole/rad^2)
$C_t - C_t - C_t$	112.7	58.4
$C_t - C_t - H_t$	110.7	37.5
$C_t - C_t - O$	107.5	59.7
$H_t - C_t - H_t$	107.8	33.0
$H_t - C_t - O$	108.9	59.0
$C_v - C_v - H_v$	120.0	40.0
$C_v - C_v - C_a$	120.0	50.0
$H_v - C_v - H_v$	120.0	40.0
$H_v - C_v - C_a$	120.0	40.0
$C_v - C_a - C_a$	120.0	50.0
$C_a - C_a - C_a$	120.0	63.0
$C_a - C_a - H_a$	120.0	35.0
$C_a - C_a - O$	121.9	43.2
$C_t - O - C_a$	108.9	49.6

Table 3. Van der Waals interaction parameters

Van der Waals interaction	D^I (kcal/mole)	ρ^I (Å)
C_t	0.066	3.50
H_t	0.030	2.50
O	0.140	2.90
C_a	0.070	3.55
H_a	0.030	2.42
C_v	0.076	3.55
H_v	0.030	2.42

Table 4. Boundary conditions for the five independent elastic properties

Property	Boundary conditions (unspecified strain components are zero)	Boundary displacements/ tractions	Strain Energy
Transverse shear modulus, G_T^f	$\varepsilon_{23} = \gamma/2$	$u_1 = 0$ $u_2 = \frac{\gamma}{2} x_3$ $u_3 = \frac{\gamma}{2} x_2$	$E^f = \frac{1}{8}\pi D^2 L G_T^f \gamma^2$
Transverse bulk modulus, K_T^f	$\varepsilon_{22} = \varepsilon_{33} = e$	$u_1 = 0$ $u_2 = e x_2$ $u_3 = e x_3$	$E^f = \frac{1}{2}\pi D^2 L K_T^f e^2$
Longitudinal shear modulus, G_L^f	$\varepsilon_{12} = \gamma/2$	$u_1 = \frac{\gamma}{2} x_2$ $u_2 = \frac{\gamma}{2} x_1$ $u_3 = 0$	$E^f = \frac{1}{8}\pi D^2 L G_L^f \gamma^2$
Longitudinal Young's modulus, Y_L^f	$\varepsilon_{11} = e$ $\sigma_{22} = \sigma_{33} = 0$	$u_1 = e x_1$ $T_2 = 0$ $T_3 = 0$	$E^f = \frac{1}{8}\pi D^2 L E_L^f e^2$
Elastic Stiffness Component, C_{11}^f	$\varepsilon_{11} = e$	$u_1 = e x_1$ $u_2 = 0$ $u_3 = 0$	$E^f = \frac{1}{8}\pi D^2 L C_{11}^f e^2$

Table 5. Effective fiber independent parameters and elastic stiffness components

G_T^f = 4.4 GPa	C_{11}^f = 457.6 GPa
K_T^f = 9.9 GPa	C_{12}^f = 8.4 GPa
G_L^f = 27.0 GPa	C_{22}^f = 14.3 GPa
Y_L^f = 450.4 GPa	C_{23}^f = 5.5 GPa
	C_{44}^f = 27.0 GPa

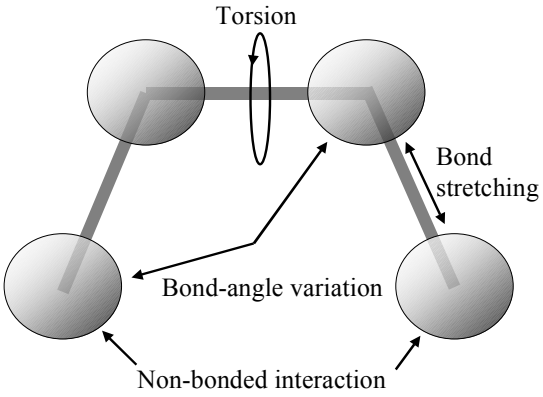

Figure 1. Molecular mechanics modeling

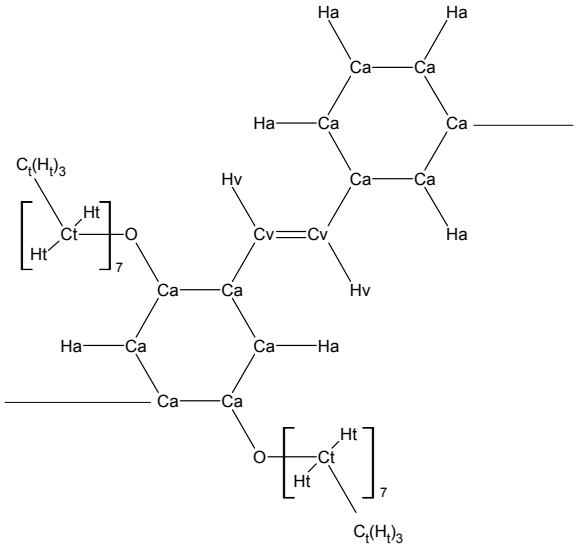

Figure 2. PmPV molecular structure

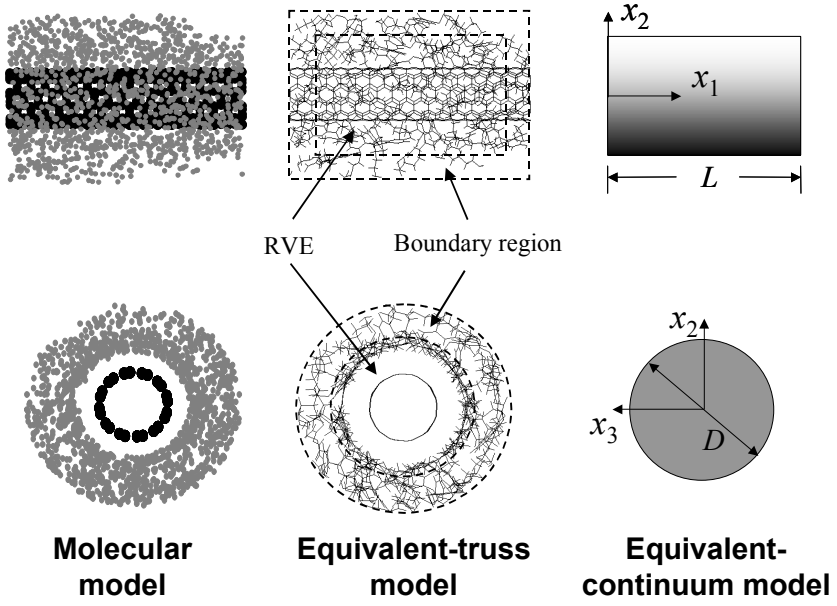

Figure 3. Equivalent-continuum modeling of effective fiber

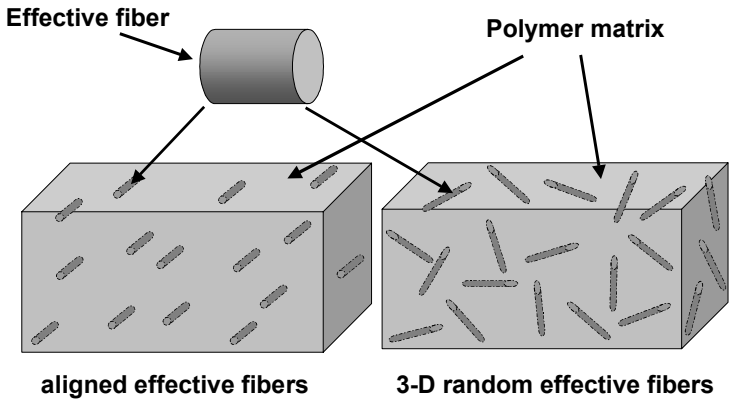

Figure 4. Orientation of effective fibers in the composite material

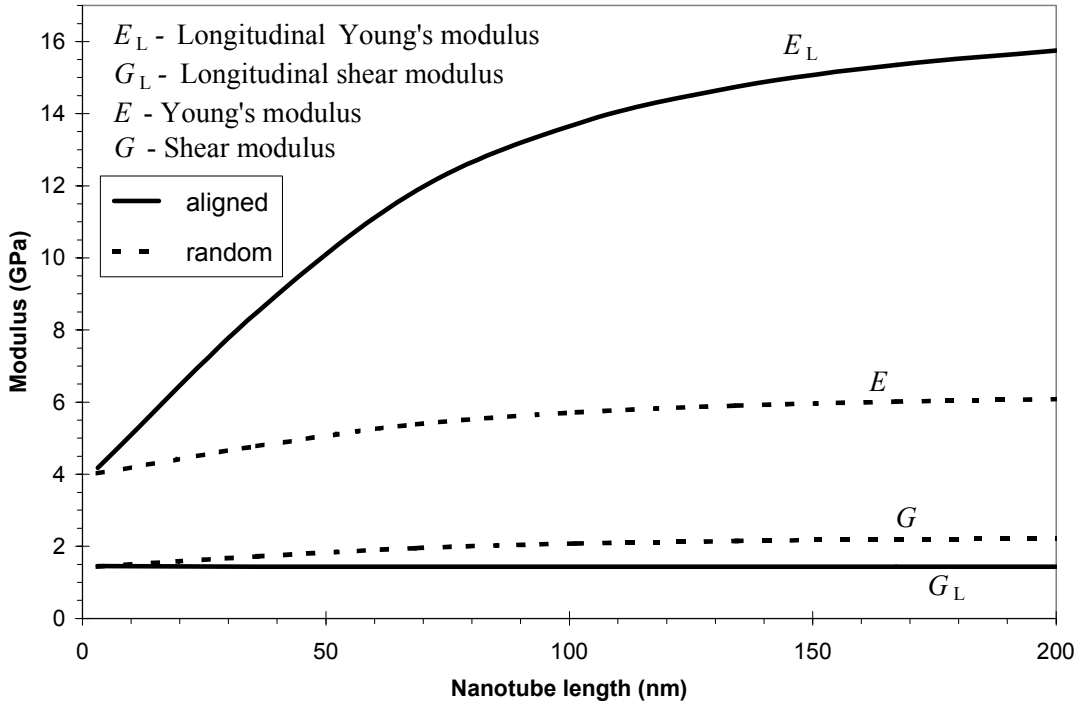

Figure 5. Modulus of aligned and random composite material vs. nanotube length

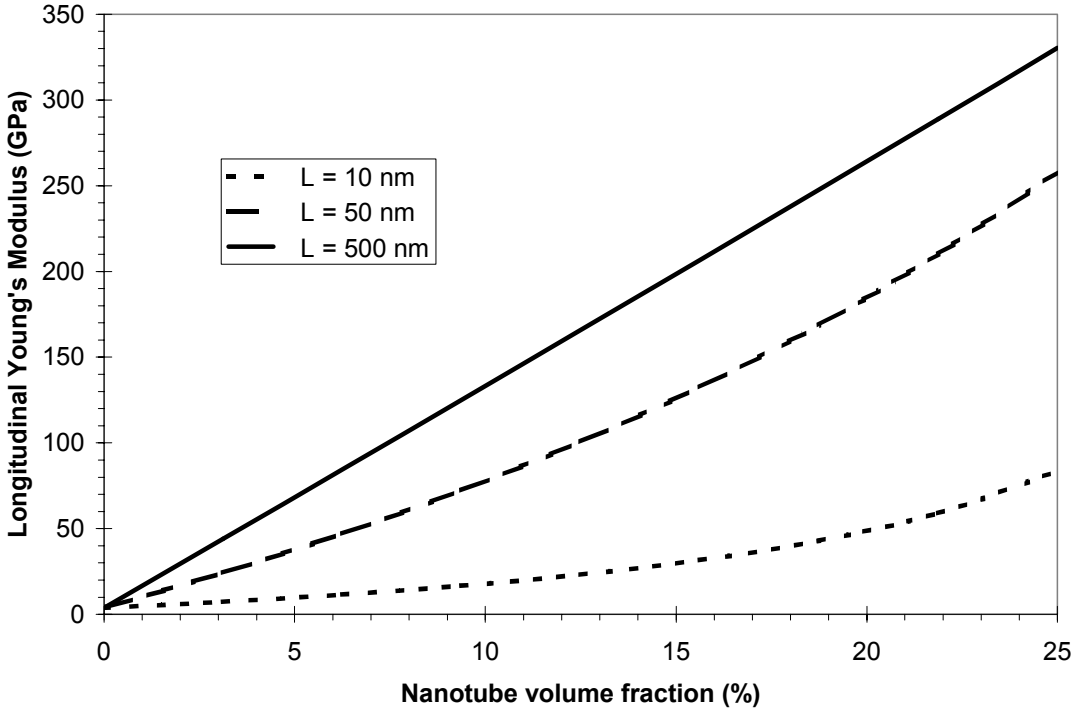

Figure 6. Longitudinal Young's modulus of aligned composite vs. nanotube volume fraction

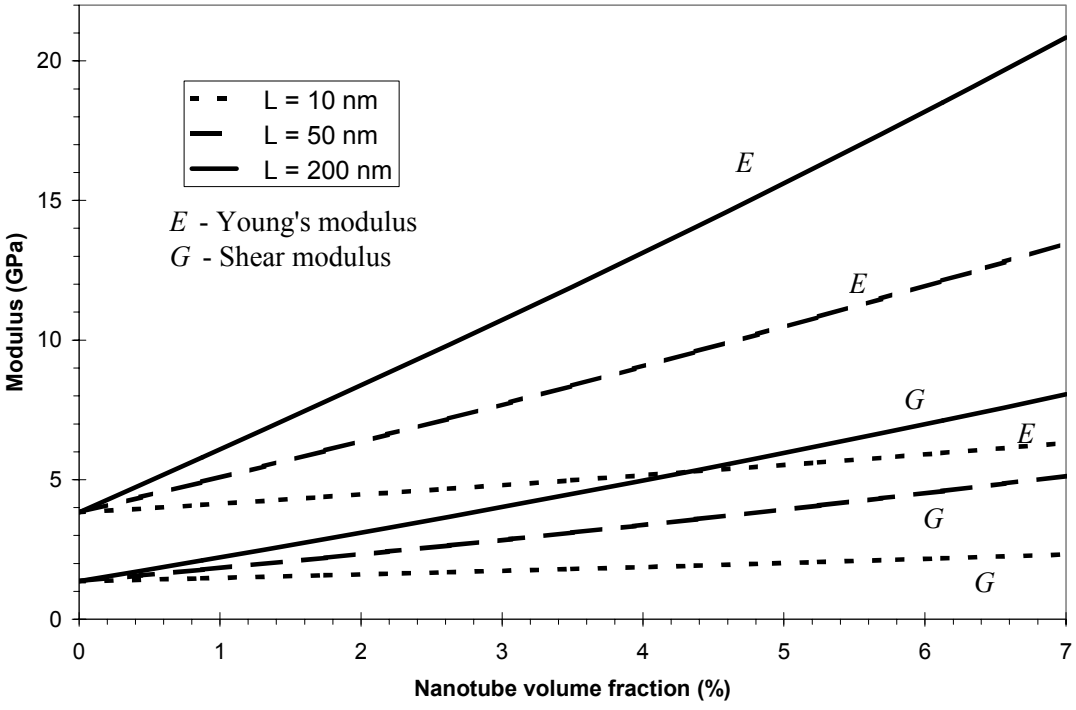

Figure 7. Modulus of random composite material vs. nanotube volume fraction